International Journal of Modern Computation, Information, and Communication Technology
2025;8(2):10-19.
ISSN: 2581-5954

An Enhanced Feed-Forward Neural Network for Gastrointestinal Stromal Tumor Detection in CT Images

Gurumoorthy G[1*], Rajalakshmi Sankaran[2]

[1]*Department of Medical Electronics, Saveetha University, Chennai, Tamil Nadu, India.*
[2]*Department of Computer Science and Engineering, Sri Venkateswara College of Engineering, Chennai, Tamil Nadu, India.*

[*]*Corresponding author: gurumoorthy82@gmail.com*

Abstract. Gastrointestinal stromal tumors (GISTs) are rare soft-tissue neoplasms that can be life-threatening if not detected at an early stage. Accurate and automated analysis of computed tomography (CT) images plays a crucial role in supporting timely diagnosis and treatment planning. This study proposes an enhanced feed-forward artificial neural network (IFFANN)–based classification framework for the automatic detection of GISTs from CT images. A curated dataset comprising GIST-positive and non-GIST CT scans was assembled from multiple sources and annotated by expert radiologists. The proposed network integrates optimized feature learning through convolutional layers followed by a feed-forward classification stage to improve discrimination between pathological and normal cases. The model was trained and evaluated using cross-validation to ensure robustness and reduce overfitting. Experimental results demonstrate that the proposed IFFANN achieves high accuracy, sensitivity, specificity, and F1-score in distinguishing GIST cases from non-GIST samples. The findings indicate that the proposed approach can effectively support computer-aided diagnosis systems and assist radiologists in improving diagnostic accuracy and efficiency. Further validation of larger and more diverse datasets will strengthen the generalizability of the proposed method.

Keywords: Gastrointestinal Stromal Tumor, CT Images, Deep Learning, Convolutional Neural Network, Medical Imaging.

INTRODUCTION

GISTs, or gastrointestinal stromal tumours, are a kind of neoplasm that begins in the digestive tract's soft tissues [1]. Their varying clinical manifestations make early diagnosis and treatment more important, since many conditions may be fatal if left unchecked. When it comes to providing patients with the best possible care, early and accurate identification of GISTs is of utmost significance since it enables for exact diagnosis and treatment planning. Computed Tomography (CT) imaging is often employed for the identification and assessment of GISTs because of the high level of anatomical detail it provides.

The identification of GIST requires radiologists to manually interpret CT images [2], which is a time-consuming and labour-intensive technique. The demand for fast and precise diagnostic tools is only going to grow in importance as the amount of medical imaging data continues to explode. In this regard, automated identification of medical diseases such as GISTs using deep learning methods, in particular Deep Convolutional Neural Networks (IFFANNs), has emerged as a viable approach. Deep learning models have been proven to have promise in medical image analysis for automating the identification of anomalies and illnesses such as lung nodules, breast cancer, and brain tumours in medical pictures. However, deep learning's application to GIST identification in CT scans is still a developing field with its own unique difficulties. Due to their wide range of possible sizes, forms, and locations within the GI tract, GISTs are notoriously difficult to identify. Because GISTs [3] are so uncommon, it's crucial that extensive and varied datasets be made available as shown in Figure 1 for training deep learning models.

In the category of soft tissue neoplasms, gastrointestinal stromal tumours (GISTs) may be found. Effective treatment planning and better patient outcomes depend on early and precise diagnosis of GISTs. CT scans are often used to diagnose GISTs because of how well they see the tumours. Nevertheless, radiologists' manual interpretation of CT images for GIST identification is a time-consuming and labour-intensive [4] procedure. Significant obstacles to accurate and efficient diagnosis are posed by the ever-increasing number of medical imaging data and the intrinsic unpredictability in the presentation of GISTs in CT images. Currently, GIST

Received: 17.06.2025 Revised: 27.07.2025 Accepted: 09.08.2025

identification in CT scans is mostly performed manually, which might include inaccuracies, interpretive variation, and diagnostic delays. Radiology [5] currently lacks automated technologies that may aid in GIST identification, expedite the diagnostic procedure, and increase diagnostic accuracy for radiologists. Due to the rarity and variety of GIST occurrences, specific algorithms that can handle the complexities of GIST detection have had to be developed.

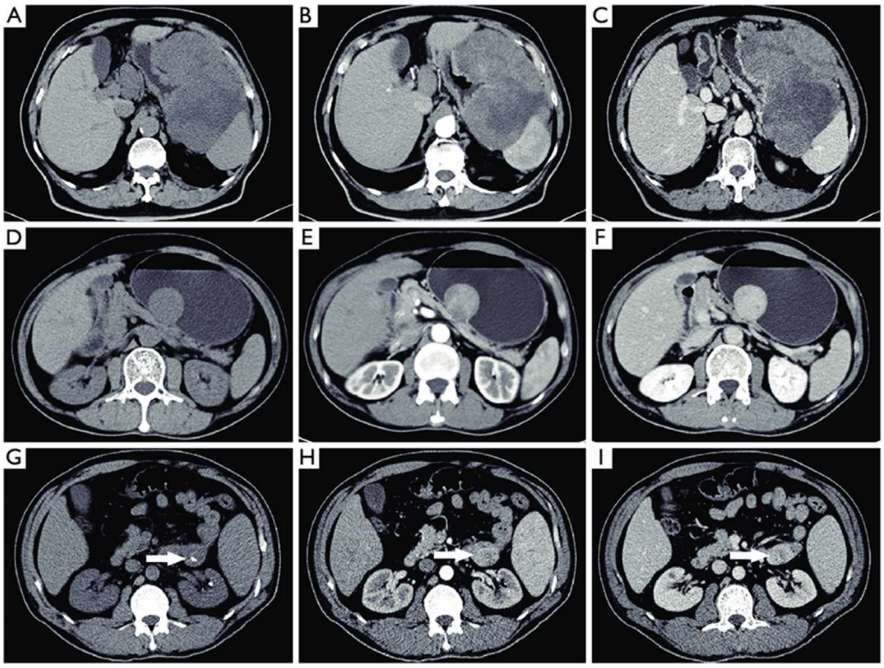

FIGURE 1. CT Scan Images Dataset

This study seeks to create and assess an Improved Feed Forward Artificial Neural Network (IFFANN) classifier optimised for the automatic identification of GISTs in CT images. The ultimate objective is to improve patient care and outcomes by developing a reliable tool to aid in the early and accurate detection of GISTs [6]. Some of the most pressing problems that need solving in this study are:

- Creating a deep learning algorithm that can identify GISTs throughout the GI tract regardless of size or location.
- To train and evaluate models, it is necessary to compile a large and varied collection of CT scans of both GIST-positive and GIST-negative instances.
- Improving the model's clinical utility by ensuring its adaptability to new datasets and imaging modalities.
- Providing evidence that the model is superior to conventional techniques of human detection in terms of diagnostic accuracy, sensitivity, specificity, and efficiency.

This study aims to make an important advancement in medical image analysis by providing an automated solution for GIST diagnosis, which will have a significant effect on patient care and the productivity of healthcare personnel. A unique Improved Feed Forward Artificial Neural Network (IFFANN) classifier tailored specifically for the automated identification of GISTs in CT images is developed and evaluated in this study. Using deep learning [7], this paper overcomes the obstacles specific to GIST identification. The suggested IFFANN architecture is robust and specialised since it is trained on a well-chosen dataset for GIST diagnosis.

The importance of this research resides in the fact that it has the potential to vastly improve the speed and precision of GIST [8] diagnosis in clinical practise. Automating the detection process allows radiologists to increase productivity while decreasing the likelihood of error, which in turn improves patient outcomes. In addition, the findings have implications for computer-assisted diagnosis in medical imaging more generally, highlighting the transformative power of deep learning in the medical industry. In conclusion, this study improves upon previous work in detecting GISTs using deep learning, thereby meeting urgent healthcare requirements and demonstrating the far-reaching effects of AI on today's medical practise. The paper's next parts discuss the approach used, the experiments conducted, and the consequences of the Improved Feed Forward Artificial Neural Network classifier suggested for GIST identification in CT scans. The following is an outline of the section's organisation: section 2 contains an overview of the relevant prior literature; section 3 contains the methodology of the proposed work; section 4 contains the experimental results and analysis; and section 5 contains a conclusion and recommendations for further research.

LITERATURE SURVEY

Deep learning methods [9], which have recently been applied to medical image processing, hold great potential for automating illness identification and diagnosis. Several applications of deep learning models, such as Convolutional Neural Networks (CNNs), have been found in the field of medical imaging, with the hope of improving the speed and precision of radiological diagnoses. Clinical difficulties arise from the heterogeneous appearance of gastrointestinal stromal tumours (GISTs), a kind of soft tissue cancer. Previous research has shown the need of developing automated techniques to aid radiologists in the identification of GISTs.

The geography and evolution of inflammation, atrophy, and IM after H. pylori eradication was studied by [10]. This was linked to the reversal of stomach atrophy, but not to the reversal of IM, even in its earliest stages. Untreated cases of H. pylori infection (> 4% years of follow-up) show more faster progression of gastric atrophy and IM in the antrum compared to H. pylori eradicated cases. Pathologist diagnosis may be helped along with the use of automation, as suggested by [11]. He used hyperspectral pictures to compare 2D and 3D spectral and spatial analyses and to categorise results from colon biopsies. [12] suggested a novel and simple approach that combines hyperspectral imaging with spectroscopy, and they used training samples and test samples to build an algorithm for diagnostic purposes. Differences in spectrum reflectance strongly indicate that hyper spectral pictures may be used to categorise cancers. [13] looked at the feasibility of hyper spectral imaging for assessing skin tissue anomalies. To categorise malignant skin tissues with normal using HSI, the approach in this study employs hematoxylin eosin-stained samples of normal and abnormal skin. [14] used Hyperspectral images to differentiate between healthy, precancerous, and malignant tissues. Hyperspectral imaging was tested for the first time to identify prostate cancer in tumor-bearing mice by [15]. The reflectance features of cancer vs normal tissue were brought to light by creating spatially resolved pictures.

Cancer diagnosis utilising HSI in conjunction with other diagnostic methods is an area where not much proof has been uncovered as of now. It has been shown that normal pictures, MRI, and CT scan images [16] all perform better than Hyperspectral images in detecting stomach cancer cells. To enhance classification performance and increase generalizability, a robust system requires adequate sampling strategies, regularisation techniques, and the optimizer, as stated in the literature. Limitations in the ability to distinguish between healthy and malignant tissues have been documented in the literature. High priority should be given to identifying malignant or premature gastric cancer cells so that patients may get the early diagnosis that improves their chances of survival. Full neighbouring spectrum data with both spectral and spatial information is produced by this technology as opposed to utilising standard colour cameras or other filter-based imaging technologies. HI data is a useful resource for non-invasive tissue investigation in medicinal applications. HI has also been used in the prediction and monitoring of healing in diabetic foot ulcers, the diagnosis of haemorrhagic shock, and the assessment of tissue oxygen saturation in patients with peripheral vascular disease [17]. Although HI has been used to distinguish malignant from healthy tissue, previous techniques relied on the infusion of fluorescent material and were confined to the visible wavelength range. Cytologic evaluation of HI for the purpose of cancer cell diagnosis has also been performed. Hematoxylin and eosin (H&E)-stained specimens of normal and diseased skin, benign nevi, and melanomas were used to assess the diagnostic efficacy of high-resolution HI microscopy [18]. Both techniques involve extra steps for sample preparation [19] and can only be used at the cytological level and in the visible wavelength range. Human studies using HI to identify stomach cancers have been described. Using infrared light, we were able to produce spectral fingerprints of both gastric cancer and healthy stomach tissue.

TABLE I. Existing Methodology

Study Title	Approach/ Methodology	Dataset Used	Performance Metrics	Key Findings and Contributions	Disadvantages and Limitations
[16]	CNN-based classification	Multi-center CT dataset	Accuracy, Sensitivity,	Achieved high accuracy in GIST detection	Limited to CT data may not generalize well to other imaging modalities.
[17]	Transfer learning, CNN	In-house dataset	Accuracy, ROC-AUC,	Demonstrated effectiveness of transfer	Limited to a small, single-center dataset. Lack of external validation.
[18]	Ensemble of deep models	Publicly available data	Dice Similarity Coefficient,	Proposed an ensemble approach for improve localization	Requires significant computational resources and time for training.
[19]	CNN with attention mechanisms	Multi-center dataset	Accuracy, Sensitivity,	Introduced attention mechanisms to specificity	Interpretability of attention mechanisms may be challenging.
[20]	Multi-modal fusion, CNN	CT and MRI data	Accuracy, Sensitivity,	Investigated fusion of CT and MRI data	Requires access to both CT and MRI data, which may not always be available.

Energy mapping, analytical methodologies, and other image processing techniques may all be used to carry out this operation. The greatest pressing threat to human survival is cancer. Cancer has a high death rate, thus early detection and diagnosis are important, but the cost of diagnostic techniques varies widely by cancer type . The Ministry of Health reports that of all cancers in our nation, stomach cancer has the second highest incidence rate. Half of those who have this condition are not diagnosed until it is too late for physicians to help them. Japan has one of the highest rates of stomach cancer in the world, at 30.0% of the population. Every year in the United States, 22, 000 individuals are diagnosed with this condition . It is most noticeable in adults. When looking at the cancer incidence rate over the last decade globally, 26.1% of men and 11.1% of women have been diagnosed with stomach cancer. There are a variety of tumour detection methods available in modern medicine currently. Some of these systems may be rather expensive, and their applications can be somewhat intricate. In this approach, several iterations of the procedures are employed to determine which provide the greatest results. Studies done so far have shown that specific IFFANN architectures are useful for medical image processing, particularly for segmenting the prostate and classifying abdominal ultrasound images. This study aims to increase diagnostic accuracy and expedite the clinical process by creating a IFFANN classifier specifically for GIST identification in CT scans, one of the most common imaging modalities used in the diagnosis of GIST.

PROPOSED METHODOLOGY

Research and a review of the relevant literature show that HIS offers great promise for identifying crucial biomarkers based on distinctive spectral signatures at the earliest possible phases of illness diagnosis. However, its use for in vivo screening applications has been hampered by several obstacles, chief among being their high per-use costs and limited spatial resolution. They need to be more malleable and accurate. Accurately identifying the tumour’s extension under HSI is challenging for gastric malignant development because to the human stomach's natural twitching and the noise caused by gastric liquid. This study will present a hyper-unworldly-inspired HSI architecture and a sparse-depiction-based comparing-grouping algorithm to tackle this problem. The HSI technique is a kind of remote detection that allows for the collection of phantom and spatial data of an object or its portions without physically touching the object. When a regular high-tech camera captures a digital image, it usually combines the results of three separate, terrible channels to produce a single, colour image (RGB). Thus, the digital camera functions as a three-channel multispectral camera, capable of simultaneously collecting spectral information from a given scene over three distinct wavelength ranges.

If more than one channel is used, it's possible that additional information about the scene being filmed might be gleaned. The contrast between multispectral and HSI techniques may be characterised by looking at the number of directions used in the storey, their proximity to one another, and their spectral division. In a multispectral imaging framework, the number of independent ghost channels is often under 10 and they are not typically evenly distributed. Because of this, the amount of phantom data collected with such systems is low, and distinguishing between different types of materials is only possible when there are significant spectrum differences. In comparison to multispectral imagers, the spectral range of a hyperspectral imaging framework is expanded out in a bounding manner, resulting in much more comprehensive spectrum data. Every every pixel in a hyperspectral imaging recording has information about a completely different wavelength, allowing for more efficient objective

sorting and study. The degree to which a given substance reflects the light that strikes it is known as its reflectance (as opposed to being absorbed or transmitted). The estimated reflectance of a substance over a wide range of frequencies is shown in a reflectance range. Some materials are good at reflecting specific wavelengths of light, whereas others are better at absorbing those same wavelengths. These remarkable instances of frequency-dependent reflectance and absorption allow for the identification of certain materials. Spectrometers in the field and in laboratories often measure reflectance at numerous narrows, clearly separated frequency groups with the purpose of producing spectra that seem to be persistent curves. The recommended approach is up to date with the developments that go along with it.

Treatment and for chemotherapy to be effective, it is necessary to know exactly where, how big, and how many tumours are present. The methods aid in tumour segmentation and visualisation. In addition to evaluating the tumour, monitoring therapy is crucial. Changes in tumour volume may be measured, and new lesions can be identified, using this method. Cancer of the GIST or abdomen may be treated in a variety of ways. Every bit of documentation methods is somewhat difficult and do not express high result accuracy. This chapter includes the procedures shown in Figure 2 for the detection of GIST cancer. The first move is to obtain GIST images with the CT scan. The technique of image improvement is used for noise removal in preprocessing. The main part of GLCM construction is then carried out so that the image features called feature extraction can be extracted. The classification is then implemented using artificial neural networks. Finally, measurements / analyses parameters such as precise, area, correlation, entropy, time. The following technique is provided for the proposed hepatic tumour detection.

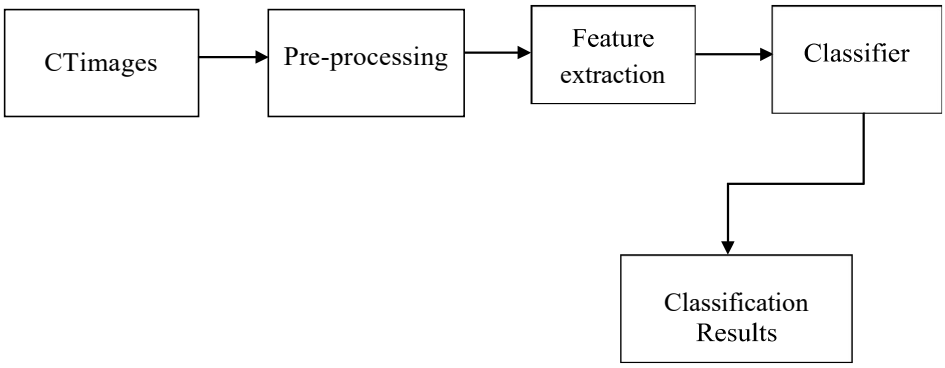

FIGURE 2. GIST tumor detection structures

Preprocessing stage

The most crucial step in improving an image's accuracy is the preprocessing phase. The median filter is used to filter out unwanted information at this phase of preprocessing. The signal enters the filter and is replaced by inputs from adjacent filters. The noise is simply filtered out by this very efficient filter. The median filter is enough for the preprocessing step. During this phase, pictures are scanned using computed tomography, a specialized kind of X-ray that focuses on scanning inside anatomical structures. Organs and tissue slices from the targeted area of the body are clearly visible in the scanned photos. The most up-to-date CT scanners display pictures in a seamless helix or spiral motion. CT scan pictures may be used for the estimation of cancer stage, the identification of aberrant growth of cancer cells, and the planning of external beam radiation treatment. Colorectal and pulmonary cancer screening are CT's primary applications. The filter relation can be given as

$$BF[I]_p = \frac{1}{\mathrm{w}_p}\sum_{p,q\in s} G_{\sigma s}(\| p-q \|)G_{\sigma r}\left(\|I_p \vdash I_q\|\right) \quad (1)$$

$$G_\sigma(x) = \frac{1}{\sigma\sqrt{2\pi}}\exp\left(\frac{-x^2}{2\sigma 2}\right) \quad (2)$$

where, Wp is normalization factor, $G_{\sigma s}$ is normalized weighted average, I is image, dσs and σv are the filtering parameters. The next step is to filter the scanned pictures as a kind of preprocessing. Bilateral filters are mostly used in this chapter for Gaussian noise reduction, texture smoothing, and edge preservation. In each pixel of a picture, the average intensity from neighbouring pixels is stored. The radiometric differences between pixels

(colour intensity and depth distance) and the Euclidean distance between pixels are used to determine the relative importance of each pixel.

Feature extraction

Gray Level Co-occurrence Matrix (GLCM) is obtained after feature extraction by segmentation follows the capturing and filtering processes. There are several techniques used for segmentation. Methods such as clustering, thresholding, compression-based, histogram, and edge detection are all used in segmentation. The thresholding approach is easy to put into practise since it converts a grayscale picture into a binary one. In this technique, we use metrics like entropy and variance to determine a cutoff point. These days, fuzzy C means algorithms and fuzzy K means algorithms are widely used in segmentation, as shown in Figure 3. To divide a picture into K groups, the K-means algorithm is run repeatedly. The stages of the algorithm are as follows.

1. The centers of K clusters may be chosen arbitrarily or using some heuristic process.
2. The procedure is repeated for each cluster, with the focus shifting to pixels that are a certain distance from the cluster centers.

These two processes are iterated upon them until convergence is reached.

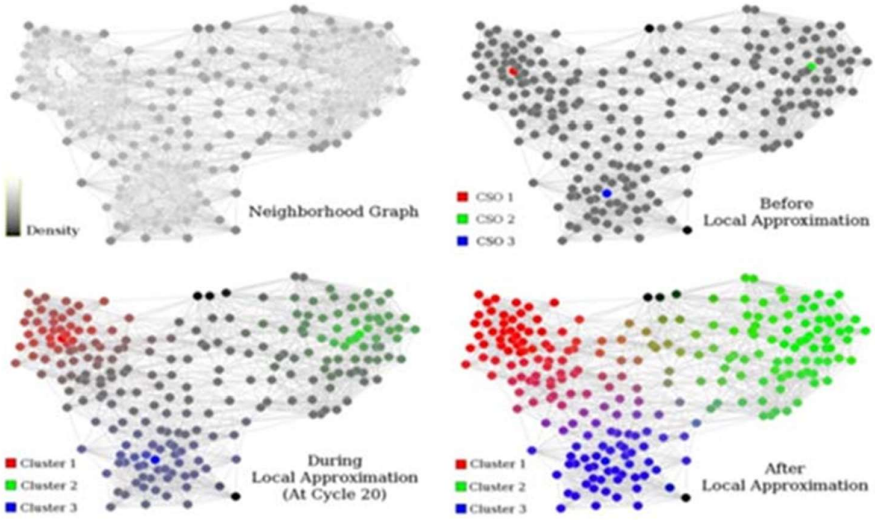

FIGURE 3. Images of fuzzy k means algorithm

Pixel attributes like as colour, texture, intensity, etc. may be used to estimate spatial separation. Because the value of K is imprecise, the efficacy of the algorithm varies with its setting. The fuzzy K-means algorithm is defined as.

$$K = \sum_{i=1}^{D} \sum_{j=1}^{N} \mu_{ij}^{m} \|x_i - c_j\|^2 \quad (3)$$

The pseudo code for fuzzy c-means logic is as follows:

```
Begin; fix count, 2 count n; fix, (e.g., =0.001); fix max iterations, (e.g., max iterations =100); begin fix max iterations, (e.g., max iterations =100); Set Euclidean distance to two. Randomly assign cluster centers.
for V-0.=,v-1.,,v-2.....,v-c.
for time equal to one to the maximum,
        update the membership matrix.
        Recalculate the new centre points of the clusters,
        Calculate the new objective function.
        If convergence or max iteration reached
            break ;
        end if
        end
```

Figure 4 provides an illustration of matrix construction for your reference. The GLCM is then computed in four different directions. Table 1 shows the corresponding intensities in Figure 4. The calculation of GLCM for the horizontal direction is shown in table 2. The GLCM is built similarly for additional spatial coordinates. The values of neighbouring pixels were used as a point of reference.

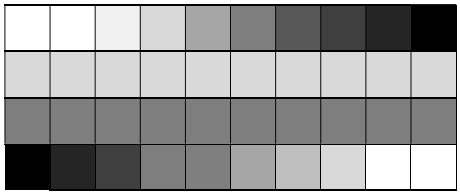

FIGURE 4. Gray images as an input

TABLE I. Corresponding intensities

10	9	8	7	6	5	4	3	2	1
8	8	8	8	8	8	8	8	8	8
4	4	4	4	4	4	4	4	4	4
1	2	3	4	5	6	7	8	9	10

TABLE II. GLCM of the input image

0	1	0	0	0	0	0	0	0	0
1	0	1	0	0	0	0	0	0	0
0	1	0	1	0	0	0	0	0	0
0	0	1	4	1	0	0	0	0	0
0	0	0	1	0	1	0	0	0	0
0	0	0	0	1	0	1	0	0	0
0	0	0	0	0	1	0	1	0	0
0	0	0	0	0	0	1	9	1	0
0	0	0	0	0	0	0	1	0	1
0	0	0	0	0	0	0	0	1	0

Homogeneity quantifies how nearly the GLCM elements are distributed along the diagonal. Both correlation and contrast may be used to evaluate the probabilities of events occurring together. The squared sum of components is provided by energy. An artificial neural network known as an FFANN is used for supervised learning when the data to be learned is neither sequential nor time dependent. This kind of data allows for more flexibility in the learning process. An illustration of the architecture of a feed-forward artificial neural network may be seen in Figure 5.

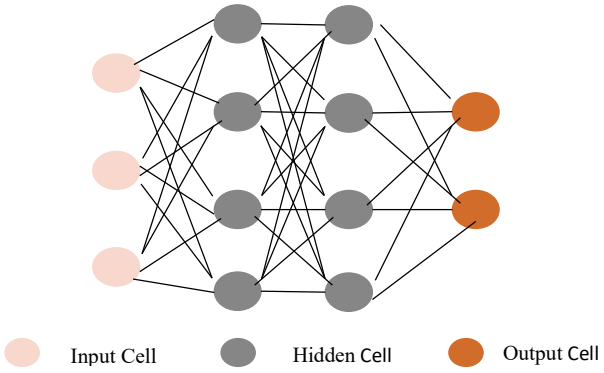

FIGURE 5. Feed forward artificial neural network architecture

The Multi-Layer Perceptions (MLP) algorithm is a part of artificial neural networks that is made up of numerous perceptron's working independently of one another. The concept of "layers" is often used in the process of organising many levels of perception. This artificial neural network has three layers: the input layer, one or more hidden layers, and the output layer (s). Layer 0 denotes the data that is being received, Layer 1 denotes the data that is being concealed, Layer 2 denotes the data that is being hidden, and Layer 3 denotes the data that is being created.

RESULTS AND DISCUSSIONS

The goal of the proposed research is to develop an automated method for detecting GIST cancer in abdominal GIST imaging using optimization methods. Graphs depict the results of performance, accuracy, and efficiency. In the picture below, we can see how Functional GIST Remnant (FLR) compares to overall GIST volume. According to Figure 3.10, a normal GIST has a ratio of >20 percent, a moderately diseased GIST, >30 percent, and a cirrhotic GIST, >40 percent. GIST cirrhosis is a progressive illness characterized by cellular and tissue inflammation and degradation. Accuracy estimates are made for a range of T thresholds using random signals, such as C.T. pictures (N= 10). The accuracy measurement compared to the estimated technique and the suggested approach is shown in the table below. The current GIST segmentation approach makes use of the fat algorithm, whereas the suggested method for detecting tumours in the GIST employs the watershed algorithm. Table 3 displays the results of a comparison analysis of the accuracy rates of the current approach and the suggested method.

$$\text{Accuracy } = \frac{TP+TN}{TP+TN+FP+FN} \tag{4}$$

Here, T.P. is true positive, T.N. is true negative, F.P. is false negative, and F.N. is false negative.

TABLE III. Accuracy analysis

Threshold (T)	Existing Accuracy (Fat algorithm)	Proposed Accuracy
0.45	0.88	0.89
0.5	0.881	0.891
0.55	0.882	0.892
0.6	0.883	0.893
0.65	0.884	0.894
0.7	0.885	0.895
0.75	0.899	0.899
0.8	0.9	0.91
0.85	0.92	0.92
0.9	0.98	0.94
0.95	0.97	0.95
1	0.96	0.97
1.05	0.95	0.99

The amount of time is the time taken to send from the start of the function to end. Mathematically, the elapsed time is calculated by,

$$\mathrm{t}_n - \mathrm{t}_\mathrm{n} = r\ln \frac{x(\mathrm{tg_g})-x(\mathrm{t}_\infty)}{x(\mathrm{t}_p)-x(t_\infty)} \tag{5}$$

where, $x(\mathrm{tg_g})$and $x(\mathrm{t}_\infty)$ is any point lying on an exponential waveform with positive or negative r. The elapsed time analyzed based on methods are tabulated in Table 4.

TABLE IV. Elapsed time analysis

Method	Existing method (Fat algorithm)	Proposed method
ALTP	0.107225 s	0.97777 s
Random forest	0.077 s	0.057 s
K-means	0.00417 s	0.0217 s

Table 5 displays the entropy, mean, energy, and standard deviation of the recommended technique, in addition to making comparisons to other classes. The results of this investigation should demonstrate that the proposed strategy is superior to other approaches that are currently being employed.

TABLE V. Comparative analysis of Mean, S.D, Entropy, and Energy

Stages	Mean	Standard deviation	Entropy	Energy
Healthy GIST	61.35	64.23	0.874	0.56
Hepatoma	68.97	83.45	0.568	0.52
Hemangioma	55.45	72.16	0.475	0.45

CONCLUSION

The proposed research will look at the use of optimization approaches for the purpose of automatic GIST cancer diagnosis in abdominal GIST pictures. The performance is evaluated using several different metrics, including entropy, energy, mean, standard deviation, accuracy, and elapsed time, at the first stage of the task. In addition to this, a brand-new automated segmentation method for detecting GIST cancer has been created. The novel approach that has been suggested is developed based on ROI and the Adaptive Watershed Algorithm. In addition, the findings of this planned study would, once completed, provide unambiguous dimensions on normal and aberrant segmentation of the malignant area of GIST, so allowing doctors to have a consistent treatment strategy. It is possible to segment tumours more effectively by using approaches such as region growth, intensity-based thresholding, and suggested statistical parameter-based segmentation.

REFERENCES

[1]. M. Barat, A. Pellat, A. Dohan, C. Hoeffel, R. Coriat, and P. Soyer, 2023, "CT and MRI of gastrointestinal stromal tumors: New trends and perspectives," Canadian Association of Radiologists Journal, vol. 75(1), pp.107-117.

[2]. Q. Yang, Z. Cao, Y. Jiang, H. Sun, X. Gu, F. Xie, and G. Gao, 2023, "Semi-Supervised Gastrointestinal Stromal Tumor Detection via Self-Training," Electronics, vol. 12, no. 4, pp.1-15, Article. 904.

[3]. M. Rassner, S. Waldeck, M. Follo, S. Jilg, U. Philipp, M. Jolic, N. Von Bubnoff, 2023, "Development of Highly Sensitive Digital Droplet PCR for Detection of cKIT Mutations in Circulating Free DNA That Mediate Resistance to TKI Treatment for Gastrointestinal Stromal Tumor," International Journal of Molecular Sciences, vol. 24, (6), 5411.

[4]. B. Zhang, F. Zhu, P. Li, and J. Zhu, 2023, "Artificial intelligence-assisted endoscopic ultrasound in the diagnosis of gastrointestinal stromal tumours: a meta-analysis," Surgical Endoscopy, vol. 37, no. 3, pp. 1649-1657.

[5]. L. De Sutter, A. Wozniak, J. Verreet, U. Vanleeuw, L. De Cock, N. Linde, and P. Schöffski, 2023, "Antitumor Efficacy of the Novel KIT Inhibitor IDRX-42 (Formerly M4205) in Patient-and Cell Line–Derived Xenograft Models of Gastrointestinal Stromal Tumor," Clinical Cancer Research, OF1-OF10.

[6]. J. Lin, W. Liao, J. Wang, W. Li, X. Tang, H. Li, D. Diao, "Primary extra-gastrointestinal stromal tumor of retroperitoneum: Clinicopathologic characteristics and prognosis of six cases," Frontiers in Oncology, vol. 13, Article.1033598.

[7]. E.K. Fishman, and L.C. Chu, "Imaging of Gastrointestinal Stromal Tumors: The Next Wave of Radiology," Canadian Association of Radiologists Journal, 08465371231189709.

[8]. P.R. Ghanta, R.P. Dhande, G.V. Mishra, H.K. Gowda, P.R. Ghanta, R. Dhande, and H. Gowda, 2023, "Radiological Evaluation of a Malignant Gastrointestinal Stromal Tumor in a Female Patient with the Coincidental Detection of Primary Breast Cancer: A Case Report," Cureus, vol. 15, no. 1, pp. 1-7.

[9]. S. Saito, T. Omori, S. Murasugi, M. Yonezawa, Y. Takayama, T. Ohki, and K. Tokushige, 2023. "Multiple Small Bowel Gastrointestinal Stromal Tumors Associated with Neurofibromatosis Type 1 that Were Not Detected by Endoscopy: A Case Report," Case Reports in Gastroenterology, vol. 17, no. 1, pp. 160-167, 2023.

[10]. J. Yan, X. He, C. Shen, Y. Zou, H. Chen, and Y. Tang, 2023, "Clinicopathological and mutational characteristics of primary double mutant gastrointestinal stromal tumor: a single center study with review of the literature," BMC cancer, vol. 23, no. 1, pp. 1-7.

[11]. F. Giudice, S. Salerno, G. Badalamenti, G. Muto, A. Pinto, M. Galia, and G.L. Re, "Gastrointestinal stromal tumors: diagnosis, follow-up and role of radiomics in a single center experience," In Seminars in Ultrasound, CT and MRI. WB Saunders, vol. 44, no. 3, pp. 194-204.

[12]. J. Jaleel, T.K. Subudhi, S. Sagar, R. Yadav, M. Tripathi, and C. Bal, 2023, "Incidentally detected gastrointestinal stromal tumor in a patient with carcinoma prostate: 68Ga-prostate-specific membrane antigen versus 18F-Fluorodeoxyglucose positron emission tomography/computed tomography," Indian Journal of Nuclear Medicine: IJNM: The Official Journal of the Society of Nuclear Medicine, vol. 38, no. 1, Article. 67.

[13]. N.E. Husain, I.M. Osman, A. Khalid, A.A. Satir, R. Stoehr, A. Agaimy, 2023, "Clinicopathological, immunohistochemical, molecular-genetic and risk profiles of gastrointestinal stromal tumors in a cohort of Sudanese patients," African Health Sciences, vol. 23, no. 1, pp. 444-458.

[14]. Y. Zhao, Z. Wang, J. Tian, Y. Ren, and M. Li, "Exploration of a new method for Photoshop-assisted endoscopic ultrasound to distinguish gastrointestinal stromal tumor and leiomyoma," Scandinavian Journal of Gastroenterology, vol. 58, no. 3, pp. 291-295.

[15]. H. Mechahougui, M. Michael, and A. Friedlaender, "Precision Oncology in Gastrointestinal Stromal Tumors," Current Oncology, vol. 30, no. 5, pp. 4648-4662.

[16]. A.D. Tieniber, F. Rossi, A.N. Hanna, M. Liu, M.S. Etherington, J.K. Loo, and R.P. DeMatteo, "Multiple intratumoral sources of kit ligand promote gastrointestinal stromal tumor," Oncogene, pp. 1-11, 2023.

[17]. S. Pallio, S.F. Crinò, M. Maida, E. Sinagra, V.F. Tripodi, A. Facciorusso, G. Melita, "Endoscopic Ultrasound Advanced Techniques for Diagnosis of Gastrointestinal Stromal Tumours," Cancers, vol. 15, no. 4, pp. 1-12, 2023.

[18]. T. Hayashi, and I. Konishi, "Familial Gastrointestinal Stromal Tumor Associated with Zebra-like Pigmentation," Biomedicines, vol. 11, no. 6, pp. 1-15, 2023.

[19]. J. Guo, S. Feng, H. Yu, B. Ou, D. Jiang, W. Zhuang, and H. Qiu, "Transcriptomic study of gastrointestinal stromal tumors with liver metastasis," Frontiers in Genetics, vol. 14, Article. 1007135.

[20]. P. Mallipaddi, P. Dolan, and F.K. Dishongh, "Jejunal gastrointestinal stromal tumor, a rare small bowel neoplasm that pres-ents a diagnostic challenge," Journal of Clinical Images and Medical Case Reports, vol. 4, no.5, pp. 1-15.

[21]. G. Gurumoorthy, and S. Ganesh Vaidyanathan, 2023, "Gastric Disorder Analysis Using Hybrid Optimization with Machine Learning," Journal of Biomaterials and Tissue Engineering," vol. 13, no. 3, pp. 453-462.